Cross-section doping topography of 4H-SiC VJFETs by various techniques

K. Tsagaraki, Maher Nafouti, H. Peyre, K Vamvoukakis, N Makris, M Kayambaki, A Stavrinidis, G Konstantinidis, M Panagopoulou, D. Alquier, et al.

Cross-section doping topography of 4H-SiC VJFETs by various techniques

K. Tsagaraki[1], M. Nafouti[2], H. Peyré[3], K. Vamvoukakis[1], N. Makris[1], M. Kayambaki[1], A. Stavrinidis[1], G. Konstantinidis[1], M. Panagopoulou[4], D. Alquier[2], K. Zekentes[1, 5,a*]

[1]MRG-IESL/ FORTH, Vassilika Vouton, PO Box 1385 Heraklion, Greece

[2]GREMAN UMR 7347, Univ. de Tours, 10 Thalès de Milet, 37071 Tours Cedex 2, France

[3]L2C, UMR 5221 CNRS-Université de Montpellier, 34095 Montpellier cedex 5, France.

[4]National Technical University of Athens, 157 80, Zografou Campus, Athens, Greece

[5]Grenoble-INP, IMEP-LAHC, F-38000 Grenoble, France

[a]zekentesk@iesl.forth.gr

Keywords: SEM, SSRM, Silicon Carbide, TSI-VJFET, SIMS, SCM.

Abstract. Different methods for cross-section doping topography of SiC Trenched-singly-implanted vertical junction field effect transistors (TSI-VJFETs) are presented with the purpose to determine the doping distribution in the epitaxial structure and the implanted areas.

Introduction

Local area doping in SiC is ensured by ion implantation and the majority of the SiC devices incorporate implanted areas. In addition, high-energy implantation up to 1MeV is employed for reaching implantation depths of 1µm. An important channeling (straggling) is observed in this case of high-energy implantation. Therefore, determination of two-dimensional implantation profile is necessary for the development of SiC devices such as TSI-VJFETs [1], which require deep (>1µm) Al implantation for the formation of the gate layer in the trenches.

Various methods have been proposed for the cross-section dopant profiling of implanted SiC such Scanning Electron Microscopy (SEM) employing a through-the-lens (ExB) detector [2, 3], Scanning Spreading Resistance Microscopy (SSRM) [4], Scanning Capacitance Microscopy (SCM) [5] or a combination of them [6].

In the present study, the results of SEM are compared with that of SCM, SSRM, Secondary Ion Mass Spectroscopy (SIMS) and finite elements simulations (TCAD Silvaco) in order to evaluate the information that can be extracted from the former method in terms of doping profiling.

Experimental

The experiments took place on pieces of processed (TSI-VJFET) SiC samples incorporating 4 epitaxial layers (#1: 1µm and n-doping: ~10^{19}cm^{-3}, #2: 1.2µm n-doping: ~10^{16}cm^{-3}, #3: 7 µm n-doping: ~$5x10^{15}$cm^{-3}, #4: 1 µm n-doping: ~$8x10^{18}$cm^{-3}) on top of a n^+ 4H-SiC substrate [1]. The TSI-VJFETs' p^+ gate area has been formed in the n^- layer #2 by Al implantation [1]. Bare witness samples have been implanted at the same time. SEM cross-sectional samples were just cleaved in air while that investigated by SCM and SSRM were mechanically polished.

Two different Field Emission Scanning Electron Microscopes have been employed for the SEM observations. The first one is a JEOL JSM-7000F featuring Everhard-Thornley detector and the second is a FEI Nova NanoSEM 230 Scanning Electron Microscope equipped with a through-the-lens detector. No major difference in the SEM contrast between p and n regions has been observed between the two microscopes on contrary to the conclusions of previous works [2]. Nevertheless, choosing an appropriate acceleration voltage is crucial in order to obtain images with optimal resolution. High-resolution images are achieved using low acceleration voltages in SEM [7] (Fig. 1) and the observations in the present study have been performed at an acceleration voltage of 1.2 kV.

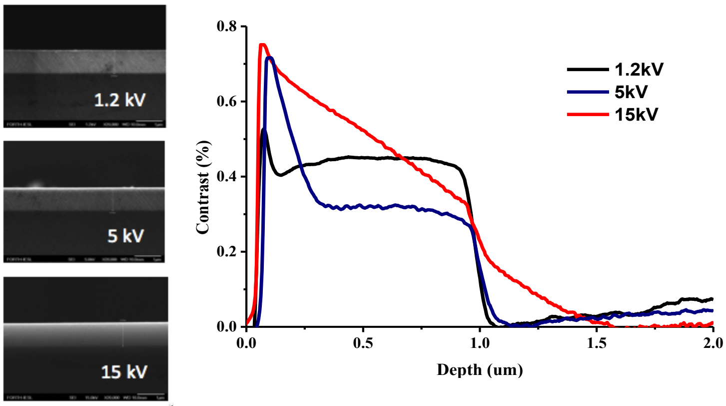

Fig. 1.Contrast versus depth. The same diode has been profiled using SEM at different acceleration voltages. As it can be seen the resolution is enhanced as the voltage drops.

For SCM and SSRM measurements, dimension V atomic force microscopy was used, coupled to a high frequency sensor (1 GHz) and to a lock-in amplifier. SCM and SSRM investigations were performed using a Pt/Ir and diamond coated silicon tip respectively. To gather the SCM signal, which is measured by employing the constant dV method, a thin oxide layer (1-2 nm) was formed over the sample. The SCM's AC signal had amplitude 4.5V at 90kHz. The Vdc bias was tuned to fix the working point around the flat band condition (depletion regime) in order to obtain a monotonic behavior of the carrier concentration as function of SCM signal. SSRM investigation was performed using a diamond coated silicon tip and under +6V DC bias.

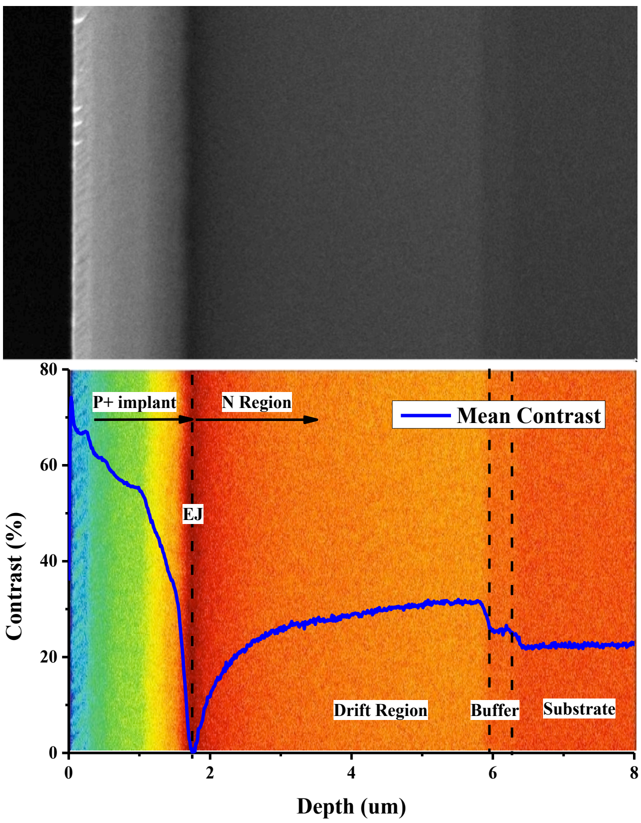

Fig. 2. SEM observations of bare epitaxial structure's cros-section. *Top*: Typical grayscale SEM photo. *Bottom:* Same photo in colorful representation. High to low SEM intensity is varied from blue to red. The contrast profile is also incorporated in the form of a curve. The image magnification is 8000x.

Results and discussion

The original SEM images were in grayscale (Fig. 1 and 2*top*). They have been converted to false color images (Fig. 2 *bottom* and Fig.3) in order to make the results more vivid. So, the background of Fig. 2 (*bottom)* and Fig. 3 are SEM images from the same bare epitaxial structure's cross-section. The contrast in both images was extracted using eq. 1 [7]:

$$\text{Contrast}= (I_x - I_{ref})/(I_x+I_{ref})\text{x}100 \quad (1)$$

where I_x is the local intensity and I_{ref} is the reference intensity, which is the minimum intensity inside the sample. Both figures show the SEM intensity profile (contrast with respect to the minimum) versus depth.

The SEM contrast is nearly 70% near the sample's surface. The contrast starts to fall as the scan progress lower until reaching a minimum (almost zero). The minimum of SEM contrast corresponds to the position of the electrical junction. Indeed, SEM intensity/contrast is correlated to the stray electric field, which is induced by the potential difference between the p and n type regions above the surface of the junction [2, 7]. The emitted secondary electrons (SE) are either accelerated or retracted from the local electric field. Therefore, the signal detected (or equivalently the contrast) is enhanced over p regions due to the higher SE intensity in comparison to the n regions. According to Fig. 2, the Electrical junction (EJ) is formed at about 1.7μm. After the minimum, a gradual increase of the contrast is observed. At about 6 μm the signal steps down due to the transition from the drift to buffer layer. A final step occurs due to the transition between the buffer and substrate.

Fig. 3 shows in addition SIMS profiles as collected from the witness samples and the corresponding TCAD Monte-Carlo simulations for the Al implantation profile according to the implantation conditions. Firstly, it can be seen that the TCAD simulation is in good agreement with SIMS measurements. Furthermore, the metallurgical junction's position (MJ), which is determined as the point where the donors' concentration becomes equal to the acceptors', is positioned in approximately 1.6μm depth in both cases. The MJ position is very close to that of EJ showing an efficient activation of the Al implanted atoms.

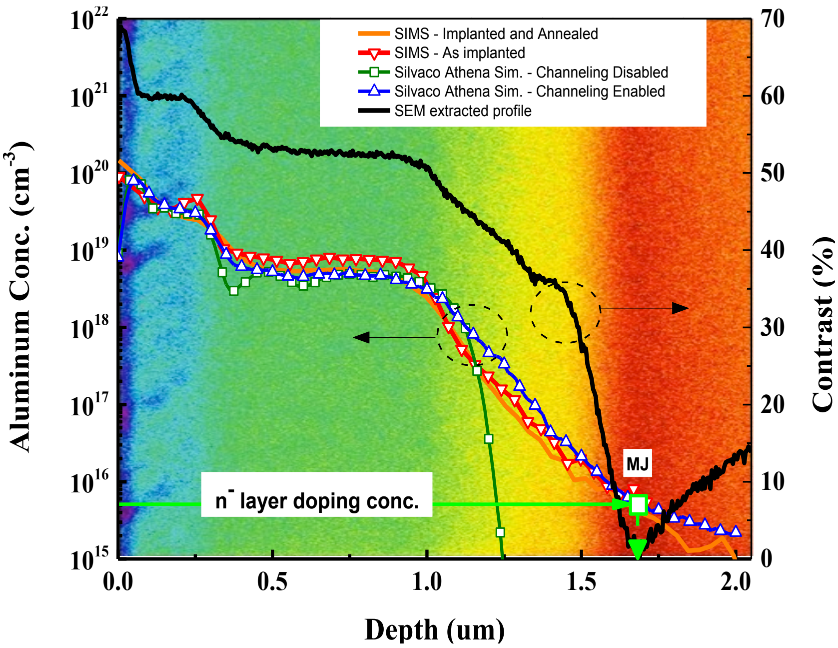

Fig. 3. SIMS, TCAD (left axis) and SEM intensity (right axis) profiles versus depth SEM profile reported on a colorful SEM image. The image magnification is 10000x.

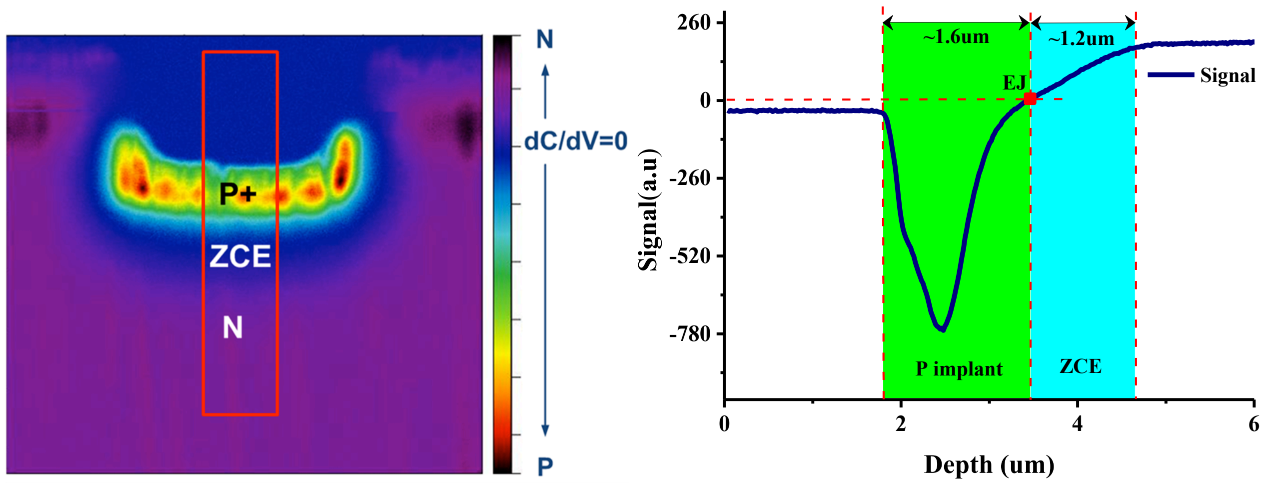

Fig. 4. SCM image of JFET's gate area (left). Quadrature Signal versus depth (right).

In the case of SCM observations, the distinction between n and p type doping is realized using signal's change of sign (for quadrature dC/dV signal, negative signal for p, positive signal for n and 0 corresponds to junction delineation). Fig.4 is a typical SCM image measured on processed samples. We used false colors in order to better recognize the different areas. The implanted area is highlighted at the center of the image with brighter colors. It can be seen that the captured SCM image is quite detailed. The space charge region (ZCE) is the blue region around the implanted region. Using the graph to the right, the implantation depth and the junction's position can be easily determined. Furthermore, the effective distance that the depletion region reaches may be extracted. After the EJ, the signal still rises up to a point where the signal becomes constant. This method could result to the extraction of the effective channel width as determined by the straggling due to the deep implantation. The EJ is at approximately 1.6 μm. This depth is almost the same with the metallurgical and electrical junction delineation determined before.

Fig. 5 shows an SSRM image from a processed sample and its signal profile collected from the gate pad area. The resolution of the image is not good enough in the gate area due to surface noise. The gate pad, on the other hand, seems to have enough area adequate for investigation. The produced graph shows the drop of the signal (resistance) due to the p implantation.

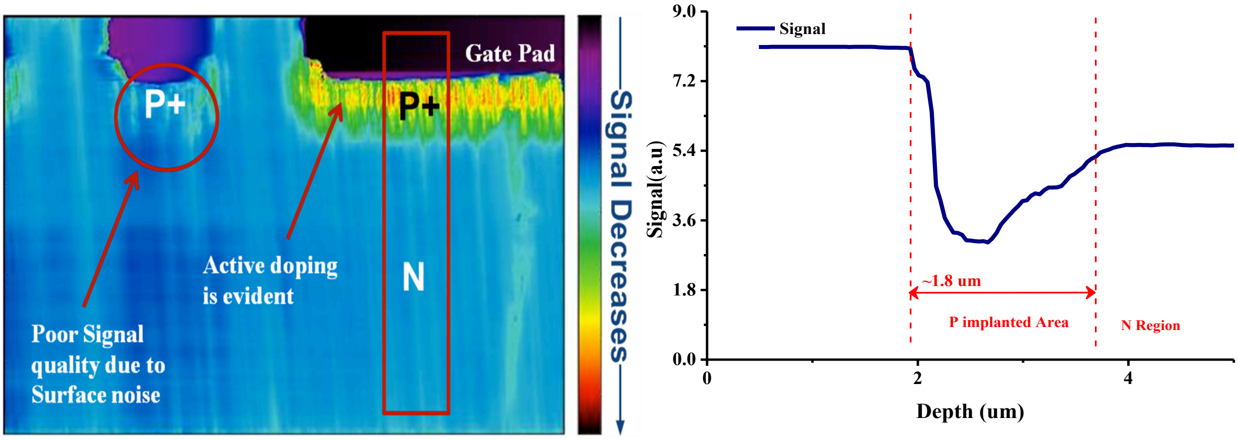

Fig. 5. SSRM image as captured near a gate pad(left). 1/R Signal versus depth (right), where R presents spreading resistance. The extension of the p-implanted area has been determined from the SCM signal (Fig.4).

Conclusions

The cross-section doping topography has been extracted using SIMS, SEM, SCM and SSRM measurements as well as TCAD simulations. From the comparison of results of the different methods, we concluded that SEM intensity profile is sufficient for determining the electrical junction position as well as the strangling due to ion implantation. There is no need of an ExB detector for making the corresponding SEM observations given that a low acceleration voltage is employed during the measurements.

Acknowledgments

Part of the work at FORTH has been funded by General Secretariat for Research and Technology (projects Anti-SiC and PROENYL). K. Zekentes acknowledges the support of European Commission through the project SICWIRE.

References

[1] K. Vamvoukakis, D. Stefanakis, A. Stavrinidis, K. Vassilevski, G. Konstantinidis, M. Kayambaki, K. Zekentes, Phys. Status Solidi A 214, No. 4, 1600452 (2017)

[2] M. Buzzo, M. Ciappa, M. Stangoni, W. Fichtner, Microelectronics Reliability 45, 1499, (2005)

[3] S. Chung, V. Wheeler, R. Myers-Ward, L. O. Nyakiti, C. R. Eddy, Jr., D. K. Gaskill, M. Skowronski, and Y. N. Picard1, J Appl. Phys., vol. 110-2011, p. 014902

[4] R. Elpelt, B. Zippelius, S. Doering, U. Winkler, Mater. Sci. Forum, 897, (2017)

[5] F. Giannazzo, L. Calcagno, F. Roccaforte, V. Raineri, Appl. Surface Sci. 184(1-4), 183 (2001)

[6] O. Ishiyama, S. Inazato, Journal of Surface Analysis 14(4), 441-443 (2008)

[7] M. Buzzo, M. Ciappa, W. Fichtner, IEEE Trans. Dev. & Mat. Reliability, 6(2), 203-212 (2006)